

Entanglement of indistinguishable particles as a probe for quantum phase transitions in the extended Hubbard model

Fernando Iemini,^{*} Thiago O. Maciel, and Reinaldo O. Vianna

Departamento de Física - ICEx - Universidade Federal de Minas Gerais, Av. Pres Antônio Carlos 6627 - Belo Horizonte - MG - Brazil - 31270-901

(Received 27 March 2015; revised manuscript received 16 July 2015; published 18 August 2015)

We investigate the quantum phase transitions of the extended Hubbard model at half-filling with periodic boundary conditions employing the entanglement of particles, as opposed to the more traditional entanglement of modes. Our results show that the entanglement has either discontinuities or local minima at the critical points. We associate the discontinuities to first-order transitions, and the minima to second-order ones. Thus we show that the entanglement of particles can be used to derive the phase diagram, except for the subtle transitions between the spin-density wave (SDW) and bond-order wave (BOW) phases and the triplet superconducting (TS) and singlet superconducting (SS) phases.

DOI: [10.1103/PhysRevB.92.075423](https://doi.org/10.1103/PhysRevB.92.075423)

PACS number(s): 05.30.Rt, 03.67.Mn, 05.50.+q, 05.30.Fk

I. INTRODUCTION

The connection between two important disciplines of physics, namely, quantum information theory and condensed matter physics, has been the subject of great interest recently, generating much activity at the border of these fields, with numerous interesting questions addressed so far [1]. In particular, the properties of entanglement in many-body systems, and the analysis of its behavior in critical systems deserve special attention.

In this work, we deal with the entanglement of indistinguishable fermionic particles in the one-dimensional extended Hubbard model (EHM). We focus on the half-filling case. The model is a generalization of the Hubbard model [2,3], which encompasses more general interactions between the fermionic particles, such as an intersite interaction, thus describing more general phenomena and a richer phase diagram. Precisely, it is given by

$$H_{\text{EHM}} = -t \sum_{j=1}^L \sum_{\sigma=\uparrow,\downarrow} (a_{j,\sigma}^\dagger a_{j+1,\sigma} + a_{j+1,\sigma}^\dagger a_{j,\sigma}) + U \sum_{j=1}^L \hat{n}_{j\uparrow} \hat{n}_{j\downarrow} + V \sum_{j=1}^L \hat{n}_j \hat{n}_{j+1}, \quad (1)$$

where L is the lattice size, $a_{j,\sigma}^\dagger$ and $a_{j,\sigma}$ are the creation and annihilation operators, respectively, of a fermion with spin σ at site j , $\hat{n}_{j,\sigma} = a_{j,\sigma}^\dagger a_{j,\sigma}$, $\hat{n}_j = \hat{n}_{j,\uparrow} + \hat{n}_{j,\downarrow}$, and we consider periodic boundary conditions (PBC), $L+1 = 1$. The hopping (tunnelling) between neighbor sites is parametrized by t , while the on-site and intersite interactions are given by U and V , respectively. Despite the apparent simplicity of the model, it exhibits a very rich phase diagram, which includes several distinct phases, namely, charge-density wave (CDW), spin-density wave (SDW), phase separation (PS), singlet (SS) and triplet (TS) superconductors, and a controversial bond-order wave (BOW). A more detailed description of the model and its phases will be given in the next section.

Our numerical analysis is performed employing the entanglement measures for indistinguishable particles introduced recently [4–6], in conjunction with the density-matrix renormalization group approach (DRMG) [7,8], which has established itself as a leading method for the simulation of one-dimensional strongly correlated quantum lattice systems. DMRG is a numerical algorithm for the efficient truncation of the Hilbert space of strongly correlated quantum systems based on a rather general decimation prescription. The algorithm has achieved unprecedented precision in the description of static, dynamic, and thermodynamic properties of one-dimensional quantum systems, quickly becoming the method of choice for numerical studies.

The paper is organized as follows. In Sec. II, we review the model and its phase diagram. In Sec. III, we present the distinct definitions of entanglement in systems of indistinguishable particles, focusing on the notion of “entanglement of particles.” In Sec. IV, we present our results. We conclude in Sec. V.

II. EXTENDED HUBBARD MODEL

In this section, we give a detailed description of the extended Hubbard model [2,3], and its distinct phases in the half-filling case. The reader familiar with the subject may skip this section.

Many efforts have been devoted to the investigation of the EHM’s phase diagram at half-filling, using both analytical and numerical methods [9–16]. Despite the apparent simplicity of the model, it exhibits a very rich phase diagram which includes several distinct phases: charge-density wave (CDW), spin-density wave (SDW), phase separation (PS), singlet (SS) and triplet (TS) superconductors, and a controversial bond-order wave (BOW). (See Fig. 1 for a schematic drawing of the phase diagram at half-filling.)

In the strong coupling limit ($|U|, |V| \gg t$), one can qualitatively characterize its phases as given by a charge-density wave, spin density wave, and a phase separation. For a strong repulsive on-site interaction ($U > 0, U \gg V$), the ground state avoids double occupancy and the spin density is periodic along the lattice, leading to an antiferromagnetic ordering, namely

^{*}fernandoiemini@gmail.com

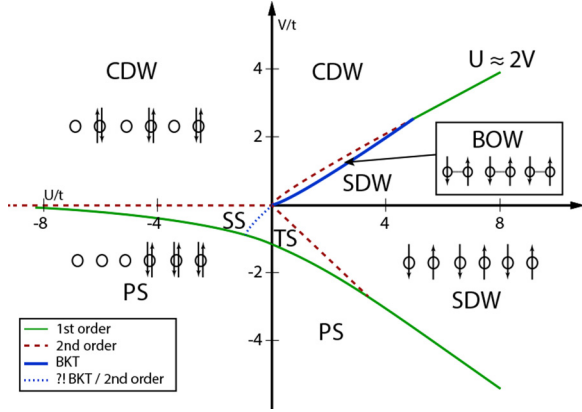


FIG. 1. (Color online) Phase diagram of the half-filled extended Hubbard model in one dimension. The distinct phases correspond to the charge-density wave (CDW), the spin-density wave (SDW), phase separation (PS), singlet (SS) and triplet (TS) superconducting phases, and bond-order wave (BOW). The order of the quantum phase transitions is identified by the different line shapes. The order of the two superconducting phases transition (blue dotted line) is controversial, being identified as a BKT transition [10], or a second-order transition [9].

spin-density wave. Its order parameter is given by

$$\mathcal{O}_{sdw}(k) = \frac{1}{L} \sum_{m,n} e^{ik(m-n)} [\langle \sigma_m^z \sigma_n^z \rangle - \langle \sigma_m^z \rangle \langle \sigma_n^z \rangle], \quad (2)$$

where $\sigma_j^z = \frac{1}{2}(\hat{n}_{j\uparrow} - \hat{n}_{j\downarrow})$. In the limit $U \rightarrow \infty$, the ground state is dominated by the following configurations:

$$|\psi\rangle_{sdw} \approx \frac{1}{\sqrt{2}} (|\uparrow, \downarrow, \uparrow, \downarrow, \dots, \uparrow_{L-1}, \downarrow_L\rangle + |\downarrow, \uparrow, \downarrow, \uparrow, \dots, \downarrow_{L-1}, \uparrow_L\rangle), \quad (3)$$

where the state is described in the real-space mode representation, in which each site can be in the following set of configurations: $\{|0\rangle, |\uparrow\rangle, |\downarrow\rangle, |\uparrow\downarrow\rangle\}$. Considering a strong repulsive intersite interaction ($V > 0$, $V \gg U$), a periodic fermionic density is generated, leading to a charge-density wave. Its order parameter is given by

$$\mathcal{O}_{cdw}(k) = \frac{1}{L} \sum_{m,n} e^{ik(m-n)} [\langle \hat{n}_m \hat{n}_n \rangle - \langle \hat{n}_m \rangle \langle \hat{n}_n \rangle]. \quad (4)$$

In the limit $V \rightarrow \infty$, the ground state is dominated by the following configurations:

$$|\psi\rangle_{cdw} \approx \frac{1}{\sqrt{2}} (|\uparrow\downarrow, 0, \uparrow\downarrow, 0, \dots, \uparrow\downarrow_{L-1}, 0\rangle + |0, \uparrow\downarrow, 0, \uparrow\downarrow, \dots, 0, \uparrow\downarrow_L\rangle). \quad (5)$$

In the range of strong attractive interactions ($U, V < 0$ or $U > 0$, $V < 0$ with $|V| \gg |U|$), the fermions cluster together, and the ground state becomes inhomogeneous, with different average charge densities in its distinct spatial regions. Such a phase is called phase separated state. In the limit $V \rightarrow -\infty$, the ground state is dominated by the following

configurations:

$$|\psi\rangle_{ps} \approx \frac{1}{\sqrt{L}} \sum_{\{\hat{\Pi}\}} \hat{\Pi} |\uparrow\downarrow, \uparrow\downarrow, \dots, \uparrow\downarrow_{(\frac{L}{2}), 0, \dots, 0}\rangle, \quad (6)$$

where $\{\hat{\Pi}\}$ is the set of translation operators.

In the weak coupling limit, different phases appear. For small attractive intersite interactions ($V < 0$), superconducting phases are raised, characterized by the pairing correlations

$$\Delta_x = \frac{1}{\sqrt{L}} \sum_j a_{j,\uparrow} a_{j+x,\downarrow}, \quad (7)$$

with the respective order parameter $\mathcal{O}_s = \sum_{x,x'} \langle \Delta_x^\dagger \Delta_{x'} \rangle$. If the on-site interactions are lower than the intersite interactions ($U \leq 2V$), the fermions will pair as a singlet superconductor, characterized by nearest-neighbor ($\Delta_{ss_{nn}}$) or on-site (Δ_{ss_o}) singlet pairing correlations given by

$$\begin{aligned} \Delta_{ss_{nn}} &= \Delta_x - \Delta_{-x} \\ &= \frac{1}{\sqrt{L}} \sum_j (a_{j,\uparrow} a_{j+x,\downarrow} - a_{j,\downarrow} a_{j+x,\uparrow}), \end{aligned} \quad (8)$$

$$\Delta_{ss_o} = \Delta_0 = \frac{1}{\sqrt{L}} \sum_j a_{j,\uparrow} a_{j,\downarrow}, \quad (9)$$

where $x = 1$. On the other hand, if the on-site interactions are higher than the intersite interactions ($U \geq 2V$), we have a triplet superconductor, characterized by nearest-neighbor triplet pairing correlations ($\Delta_{ts_{nn}}$) given by

$$\begin{aligned} \Delta_{ts_{nn}} &= \Delta_x + \Delta_{-x} \\ &= \frac{1}{\sqrt{L}} \sum_j (a_{j,\uparrow} a_{j+x,\downarrow} + a_{j,\downarrow} a_{j+x,\uparrow}), \end{aligned} \quad (10)$$

where $x = 1$.

Note that the difference between the singlet and triplet pairing correlations is simply a plus or minus sign. It can be clarified if we consider, for example, the case of two fermions in a singlet or triplet spin state, given by $(|ij\rangle \pm |ji\rangle)(|\uparrow\downarrow\rangle \mp |\downarrow\uparrow\rangle)$. Expanding this state, we have

$$\begin{aligned} &(|ij\rangle(|\uparrow\downarrow\rangle \mp |\downarrow\uparrow\rangle) \pm |ji\rangle(|\uparrow\downarrow\rangle \mp |\downarrow\uparrow\rangle)) \\ &= |i\uparrow, j\downarrow\rangle \mp |i\downarrow, j\uparrow\rangle \pm |j\uparrow, i\downarrow\rangle - |j\downarrow, i\uparrow\rangle \\ &= (|i\uparrow, j\downarrow\rangle - |j\downarrow, i\uparrow\rangle) \mp (|i\downarrow, j\uparrow\rangle - |j\uparrow, i\downarrow\rangle) \\ &= (a_{i\uparrow}^\dagger a_{j\downarrow}^\dagger \mp a_{i\downarrow}^\dagger a_{j\uparrow}^\dagger) |\text{vac}\rangle, \end{aligned} \quad (11)$$

where the lower/upper sign corresponds to the singlet/triplet pairing correlation.

The last phase in the diagram is the controversial bond-order wave (BOW). By studying the EHM ground-state broken symmetries, using level crossings in excitation spectra, obtained by exact diagonalization, Nakamura [10] argued for the existence of a novel bond-order-wave phase for small to intermediate values of positive U and V , in a narrow strip between CDW and SDW phases. This phase exhibits alternating strengths of the expectation value of the kinetic energy operator on the bonds, and is characterized by the

following order parameter:

$$\mathcal{O}_{\text{bow}}(k) = \frac{1}{L} \sum_{m,n} e^{ik(m-n)} [\langle B_{m,m+1} B_{n,n+1} \rangle - \langle B_{m,m+1} \rangle \langle B_{n,n+1} \rangle], \quad (12)$$

where $B_{m,m+1} = \sum_{\sigma} (a_{m,\sigma}^{\dagger} a_{m+1,\sigma} + \text{H.c.})$ is the kinetic energy operator associated with the m th bond. Nakamura argued that the CDW-SDW transition is replaced by two separate transitions, namely: (i) a continuous CDW-BOW transition and (ii) a Berezinskii-Kosterlitz-Thouless (BKT) spin-gap transition from BOW to SDW. Such remarkable proposal was later confirmed by several works [11–16], employing different numerical methods, like DMRG, Monte Carlo or exact diagonalization. Nevertheless, while the BOW-CDW phase boundary can be well resolved, since it involves a standard second-order (continuous) phase transition, the SDW-BOW boundary is more difficult to locate, for it involves a BKT transition in which the spin gap opens exponentially slowly as one enters the BOW phase. The precise location of the BOW phase is then still a subject of debate. To the best of our knowledge, the best estimates for the transitions, taking $U/t = 4$, correspond to a CDW-BOW transition at $V/t \approx 2.16$ [11,12,15,16], and to a BOW-SDW transition in the range $V/t \approx 1.88\text{--}2.00$ [11,12,15,16], or $V/t = 2.08 \pm 0.02$ [13].

III. ENTANGLEMENT OF INDISTINGUISHABLE PARTICLES

Despite widely studied in systems of distinguishable particles, entanglement or more general notions of quantum correlations have received less attention in the case of indistinguishable particles. In this case, the space of quantum states is restricted to symmetric (\mathcal{S}) or antisymmetric (\mathcal{A}) subspaces, depending on the bosonic or fermionic nature of the system, and the particles are no longer accessible individually, thus eliminating the usual notions of separability and local measurements, and making the analysis of correlations much subtler. In fact, there are a multitude of distinct approaches and an ongoing debate around the entanglement in these systems [6,17–30]. Nevertheless, despite the variety, the approaches consist essentially in the analysis of correlations under two different aspects: the correlations genuinely arising from the entanglement between the particles (entanglement of particles) [6,17–24], and the correlations arising from the entanglement between the modes of the system (entanglement of modes) [25–28]. These two notions of entanglement are complementary, and the use of one or the other depends on the particular situation under scrutiny. For example, the correlations in eigenstates of a many-body Hamiltonian could be more naturally described by entanglement of particles, whereas certain quantum information protocols could prompt a description in terms of entanglement of modes. Once one has opted for a certain notion of entanglement, there are interesting methods to quantify it [4–6,31–34].

Entanglement of modes can be understood by mapping the quantum state in its number representation, namely,

$$\begin{aligned} a_{j_1}^{\dagger} \dots a_{j_N}^{\dagger} |\text{vac}\rangle &\longrightarrow |0 \dots 1_{j_1} \dots 1_{j_N} \dots 0\rangle, \\ \hat{\mathcal{A}}(\mathcal{H}_1^M \otimes \dots \otimes \mathcal{H}_N^M) &\longrightarrow (\mathcal{H}_1^2 \otimes \dots \otimes \mathcal{H}_M^2), \end{aligned} \quad (13)$$

where $j_i = 1, \dots, M$, and $\{a_j^{\dagger}\}_{j=1}^M$ is an arbitrary set of M fermionic operators describing the single-particle modes of the system (not necessarily the real-space modes as in the Hamiltonian definition). We will denote hereafter as ‘‘configuration representation (number representation)’’ the left (right) side of the previous equation. Such equation corresponds to a mapping to distinguishable qubits, represented by the occupied ($|1\rangle_j$) or unoccupied ($|0\rangle_j$) modes, which then allows one to employ all the tools commonly used in distinguishable quantum systems in order to analyze their correlations. One could, for example, use the von Neumann entropy of the reduced state representing a block with ℓ modes, in order to quantify the entanglement between this block with the rest of the modes. The reduced state is obtained by the partial trace in the number representation ($\rho_{\ell} = \text{Tr}_{j \notin \ell}(|\psi\rangle\langle\psi|)$). Notice that, in the mode representation, *local* observables may actually involve correlations between particles. For example, in the Hubbard model, although the operator ‘‘ $a_{j\uparrow}^{\dagger} a_{j\downarrow}^{\dagger} a_{j\downarrow} a_{j\uparrow}$ ’’ acts locally at the j th site (real-space modes), it describes pairing correlations between particles. The algebra of local observables at the modes, defined in the number representation, is generated by

$$\begin{aligned} \Omega_{\text{loc}} &= \{\hat{\mathcal{O}}_1 \otimes \mathcal{I}_{2,M}; \mathcal{I} \otimes \hat{\mathcal{O}}_2 \otimes \mathcal{I}_{3,M}; \dots \dots; \\ &\mathcal{I}_{1,(M-1)} \otimes \hat{\mathcal{O}}_M \parallel \hat{\mathcal{O}}_j^{\dagger} = \hat{\mathcal{O}}_j\}, \end{aligned} \quad (14)$$

where $\mathcal{I}_{i,j} \equiv \mathcal{I}_i \otimes \mathcal{I}_{i+1} \otimes \dots \otimes \mathcal{I}_j$, with $j > i$ and \mathcal{I}_i is the identity operator acting on mode i . In this way, unentangled states are those that can be completely described by such local observables. It is known that such states are simply the separable states in the usual tensor product form, $|\psi\rangle_{\text{un}} = |\phi_1\rangle \otimes |\phi_2\rangle \dots \otimes |\phi_M\rangle$.

Based on the previous reasoning, we now define the notion of *entanglement of particles*. Notice first that one cannot analyze the system under the usual paradigm of *separability and locality*, where the reduced states obtained by partial trace are mixed ($\rho_r = \text{Tr}_{2\dots N}(|\psi\rangle\langle\psi|)$), whenever the global state is pure and entangled. Therefore, in the case of indistinguishable particles in the configuration representation, the use of partial trace to characterize entanglement should be carefully reviewed, since it would suggest that all pure fermionic states are entangled, given that their reduced states are always mixed. In order to generalize the notion of entanglement for systems of indistinguishable particles, the approach based on the algebra of observables sheds light on the problem and allows us to go beyond the paradigm of separability and locality.

We now define the proper algebra of ‘‘local observables’’ as the one composed by operators which do not create correlations between the indistinguishable particles. Such algebra, defined in the configuration representation, is generated by the following single-particle operators:

$$\begin{aligned} \Omega_{\text{loc}} &= \{\hat{\mathcal{O}} \otimes \mathcal{I}_{2,N} + \mathcal{I} \otimes \hat{\mathcal{O}} \otimes \mathcal{I}_{3,N} + \dots \dots \\ &+ \mathcal{I}_{1,(N-1)} \otimes \hat{\mathcal{O}} \parallel \hat{\mathcal{O}}^{\dagger} = \hat{\mathcal{O}}\}, \end{aligned} \quad (15)$$

where N is the number of particles. Equivalently, using the second quantization formalism, the above set is given by the number conserving quadratic operators, $\Omega_{\text{loc}} = \{(a_i^{\dagger} a_j + \text{H.c.}) | i, j = 1, \dots, M\}$. The states that can be completely described by such algebra form, in this way, the set of unentangled states, where any particle is not entangled with any

other. Intuitively, we would expect that this set corresponded to single Slater determinants with fixed particle number. More precisely, for a system with N fermions, it is given by

$$|\psi\rangle_{\text{un}} = a_{j_1}^\dagger a_{j_2}^\dagger \dots a_{j_N}^\dagger |\text{vac}\rangle, \quad (16)$$

where $\{a_j^\dagger\}$ is an arbitrary set of fermionic operators. Recall that these operators cannot be quasiparticles with particle-hole superpositions, as usual in a Bogoliubov transformation, since the above states have a fixed number of fermions. In fact, distinct approaches confirmed that such set does indeed correspond to the unentangled states [6,17–24]. The only nonclassical correlation present in such states is the *exchange*, due to the antisymmetrization, which does not constitute entanglement. For example, in Ref. [17], the analysis follows by using a very elegant mathematical formalism, called GNS (Gelfand-Naimark-Segal) construction, for the case of two fermions, each one with Hilbert space dimension 3 or 4, and two bosons with dimension 3; in Refs. [23,24] the authors propose a “generalized entanglement (GE)” measure, obtaining a simple formula for the “partial trace,” and the set of fermionic unentangled states for an arbitrary number of particles; or also in Ref. [6], where a general notion of quantum correlation beyond entanglement (the *quantumness* of correlations) is investigated by means of an “activation protocol,” which yields the same set of states with no *quantumness* as the above unentangled one.

As in the case of distinguishable modes, the von Neumann entropy also provides a good quantifier for the entanglement of indistinguishable particles. We can define the shifted von Neumann entropy of entanglement [4] as follows:

$$E_p(|\psi\rangle\langle\psi|) = S(\rho_r) - \log_2 N, \quad (17)$$

where $\rho_r = \text{Tr}_1 \dots \text{Tr}_{N-1}(|\psi\rangle\langle\psi|)$ is the single-particle reduced state, the partial trace is taken in the configuration space, and $S(\rho) = -\text{Tr}(\rho \log_2 \rho)$ is the von Neumann entropy. Such a quantifier is obtained simply by noticing that each extremal state in the one-particle reduced space is respective to a unique single Slater determinant [35]. More precisely, the single-particle reduced state of a single Slater determinant [as Eq. (16)] is given by

$$\rho_r = \frac{1}{N} \sum_{i=1}^N a_{j_i}^\dagger |\text{vac}\rangle\langle\text{vac}| a_{j_i} \quad (18)$$

and its particle entanglement is null, $E_p(|\psi\rangle\langle\psi|) = 0$. If the state cannot be described by a single Slater determinant, its entanglement is necessarily non null, $E_p(|\psi\rangle\langle\psi|) > 0$, and at least one of its particles is entangled with another one. Maximally entangled states have their single-particle reduced states described by the maximally mixed state, as, for example, the strong coupling limit phases SDW, CDW, and PS, as described in Eqs. (3), (5), and (6), respectively, whose reduced state is given by

$$\rho_r = \frac{1}{2L} \sum_{j=1}^L \sum_{\sigma=\uparrow,\downarrow} a_{j,\sigma}^\dagger |\text{vac}\rangle\langle\text{vac}| a_{j,\sigma}, \quad (19)$$

which have maximal von Neumann entropy, $S(\rho_r) = \log_2(2L)$, and consequently maximal particle entanglement, $E_p(|\psi\rangle\langle\psi|) = 1$.

If the Hamiltonian has certain symmetries, its ground-state entanglement can be analytically calculated as a simple function of its quadratures [4]. In our particular case, from both \hat{S}_z and translational symmetries in the extended Hubbard model, formally given by

$$\text{Tr}(a_{i\sigma}^\dagger a_{j\bar{\sigma}} \rho_g) = 0, \quad \forall i, j, \quad (20)$$

$$\text{Tr}(a_{i\sigma}^\dagger a_{j\sigma} \rho_g) = \text{Tr}(a_{(i+\delta)\sigma}^\dagger a_{(j+\delta)\sigma} \rho_g), \quad (21)$$

where $a_{j\sigma}^{(\dagger)}$ is the annihilation (creation) fermionic operator of a particle in the j th site, with spin σ , and $\rho_g = |g\rangle\langle g|$ is the ground state of the Hamiltonian, we have that its single-particle reduced state $(\rho_r(i\sigma, j\bar{\sigma}) = \frac{1}{N} \text{Tr}(a_{j\bar{\sigma}}^\dagger a_{i\sigma} \rho_g))$ is disjoint in the subspaces with distinct spin, $\rho_r = \rho_r^{\sigma=\uparrow} \oplus \rho_r^{\sigma=\downarrow}$, and each of these terms is given by a circulant matrix

$$\rho_r^\sigma = \frac{1}{N} \begin{pmatrix} x_0 & x_1 & \dots & x_{L-2} & x_{L-1} \\ x_{L-1} & x_0 & x_1 & & x_{L-2} \\ \vdots & x_{L-1} & x_0 & \ddots & \vdots \\ x_2 & & \ddots & \ddots & x_1 \\ x_1 & x_2 & \dots & x_{L-1} & x_0 \end{pmatrix}, \quad (22)$$

$$x_\delta = \langle a_{(j+\delta)\sigma}^\dagger a_{j\sigma} \rangle, \quad (23)$$

where L is the lattice size. In this way the matrix is easily diagonalized, and its eigenvalues $\{\lambda_k^\sigma\}$ are given by a Fourier transform of the quadratures:

$$\lambda_k^\sigma = \frac{1}{L} \sum_{\delta=0}^{L-1} e^{ik\delta} x_\delta, \quad k = \left[0, \frac{2\pi}{L}, \dots, (L-1)\frac{2\pi}{L}\right]. \quad (24)$$

The entanglement is then directly obtained from Eq. (17).

IV. ENTANGLEMENT AND QUANTUM PHASE TRANSITIONS

The computation of the single-particle correlations, and consequently the entanglement of particles, was numerically performed using DMRG. Although DMRG is less accurate for problems with periodic boundary conditions (PBC) than with open boundary conditions (OBC), from the physical viewpoint PBC are strongly preferable over OBC, as boundary effects are eliminated and finite size extrapolations can be performed for much smaller system sizes. In this work, we analyze the extended Hubbard model considering PBC. Our simulations were performed for systems up to $L = 352$ sites, always keeping a large enough dimension (m) for the renormalized matrices (ranging from $m = 100$ to 1000) and number of sweeps (~ 20 sweeps), in order to obtain an accurate precision. In Fig. 2, we see that m ranging from 200 to 300 is enough for an entanglement accuracy of the order of $\mathcal{O}(10^{-4})$. The accuracy for the ground-state energy, as well as the truncation error, using such parameters, are of the order of $\mathcal{O}(10^{-7})$.

Our results for the entanglement of particles in the extended Hubbard model at half-filling are shown in Fig. 3, to be dissected below. It is remarkable that such picture highlights the known phase diagram of the model. We first note that, as

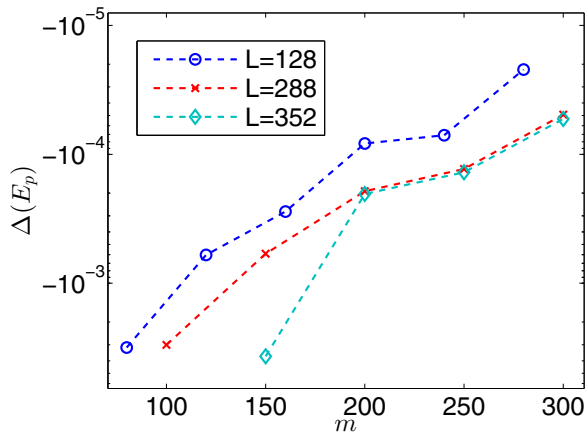


FIG. 2. (Color online) Accuracy analysis for the computation of entanglement of particles using DMRG. It shows the accuracy of the entanglement, $\Delta(E_p) = E_p(m) - E_p(m - 50)$, as a function of m (dimension of the renormalized matrices), at the point $U = 4$, $V = 2.11$, and using 20 sweeps in the computation, which is enough for the ground-state convergence.

expected, we have a maximum of entanglement at the strong coupling limits ($E_p \rightarrow 1$), and as we decrease the interactions between the particles, the entanglement tends also to decrease, until the unentangled case for the noninteracting Hamiltonian ($U = V = 0$). The figure thus presents the shape of a valley around this point. Following then the discontinuities and the local minimum points in the entanglement, we can easily identify the quantum phase transitions, except for both the subtle SDW-BOW transition, and the transition between the superconductor phases TS-SS. In the former case, one needs to recall that the observation of the BOW phase is by itself

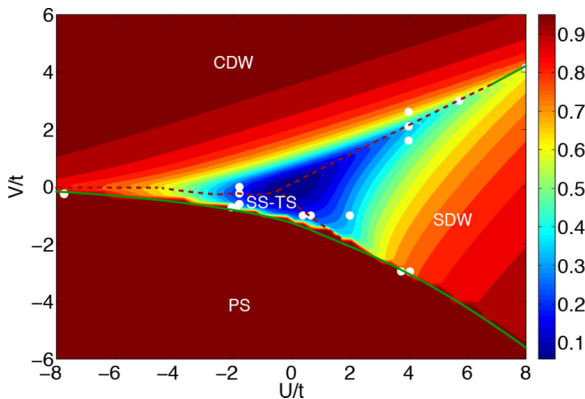


FIG. 3. (Color online) Contour map for the entanglement of particles “ E_p ” as a function of the interaction terms V/t and U/t , in a system with $L = 128$ sites at half-filling. The entanglement behavior in the thermodynamic limit, $L \rightarrow \infty$, keeping fixed the filling $n = N/L = 1$, is qualitatively the same, with slight differences of the order of $\mathcal{O}(10^{-2})$ in its magnitude; see Appendix for a detailed discussion. The (green) continuous line denotes the discontinuity at the entanglement function, while the (red) dashed line denotes the local minima. The white dots correspond to the points where we performed a detailed finite-size scaling analysis (see Table I in Appendix).

a hard task, since its gap opens exponentially slowly, and also that there are evidences that such transition is of infinite order [36,37]. Therefore we believe that a possible detection of such transition by the entanglement of particles would require higher precision numerical analysis as well as the study of larger lattice sizes. Concerning the TS-SS transition, on the one hand the order of the two superconducting phases transition is controversial, being identified as a BKT transition [10] as well as a second-order one [9] in the literature. On the one hand, we would be led to strengthen the result of a BKT transition, since our entanglement does not detect it. On the other hand, the apathy of the entanglement of particles on distinguishing the two phases is reasonable, since the correlations between the particles in the two superconducting phases have essentially the same characteristics. Thus it is hard to precisely conclude the reason for the failure to detect such a transition with our measure of entanglement.

The discontinuities in the entanglement are directly identified with the first-order quantum phase transitions, whereas the minimum points are identified with the second-order quantum phase transitions. When crossing a first-order transition, the ground-state energy presents a discontinuity and consequently also its observables present a discontinuity. In this way, the eigenvalues “ λ_k ” of the single-particle reduced density matrix [Eq. (24)], and the entanglement obtained from them, should present a discontinuity. The occurrence of the minimum points is due to the divergence of the correlation length when approaching the second-order transitions. As described in the previous section, the eigenvalues “ λ_k ” are given in momentum space by the Fourier transform of the real-space quadratures “ $\langle a_{j\sigma}^\dagger a_{l\sigma} \rangle$ ” [Eq. (24)]. In this way, if we are close to the transitions, such real-space quadratures tend to become delocalized or spread out along the lattice, thus leading to more localized eigenvalue distributions in momentum space, and consequently to smaller von Neumann entropies. It is worth remarking that such behavior is the opposite of the entanglement of modes, where the sites are maximally entangled at the second-order transitions. As an example, see in Fig. 4 the eigenvalue distribution for a system with $L = 128$ sites when crossing the BOW-CDW quantum phase transition.

We present now the entanglement behavior in some specific slices of the phase diagram with $L = 128$, in order to clarify the above discussion and results. More specifically, we show the entanglement behavior in the PS-SS-CDW, PS-SS-SDW, and PS-SDW-CDW transitions. Notice that our finite-size scaling analysis showed that in the thermodynamic limit the entanglement behavior is qualitatively similar (see Appendix), with a scaling inversely proportional to the lattice size, $E_p = aL^{-1} + b$, where a and b are constants.

A. PS-SS-CDW

In Fig. 5, we see the entanglement behavior across the PS-SS-CDW phases. We clearly see, for any fixed attractive onsite interaction ($U/t < 0$), a discontinuity in the entanglement followed by a local minimum point, as we increase the value of the intersite interactions V/t . The discontinuity is related to the first-order transition PS-SS, while the local minimum is related to the second-order transition SS-CDW. We see,

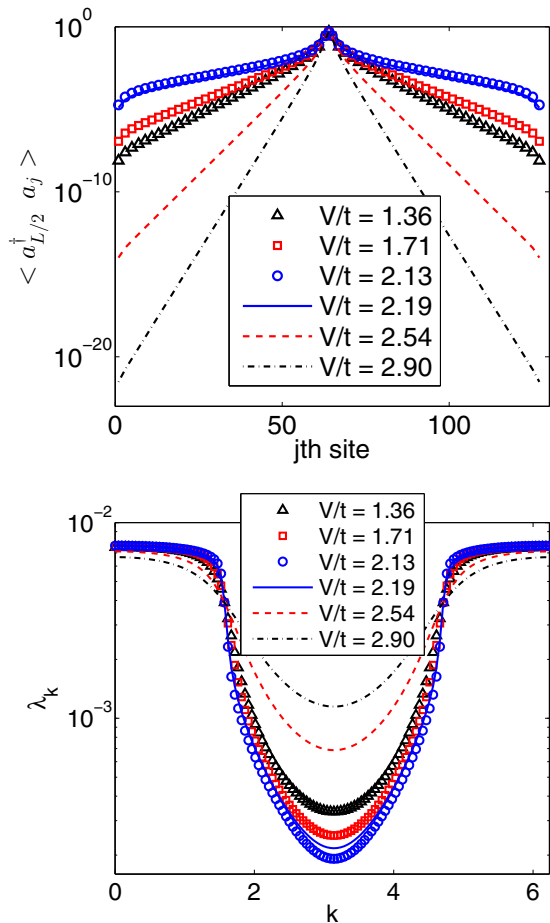


FIG. 4. (Color online) (Top) Single-particle quadratures “ $\langle a_{L/2}^\dagger a_j \rangle$ ” along the lattice sites, and (bottom) eigenvalue distribution “ λ_k ” for the single-particle reduced state in a fixed spin sector, as given in Eq. (24). We consider a fixed $U/t = 4$. The vertical axis is in logarithmic scale, in order to make clearer the visualisation. As we approach the BOW-CDW quantum phase transition point, at $V/t \approx 2.13$, we see that the quadratures tend to delocalise along the lattice, whereas the eigenvalue distribution becomes more localized.

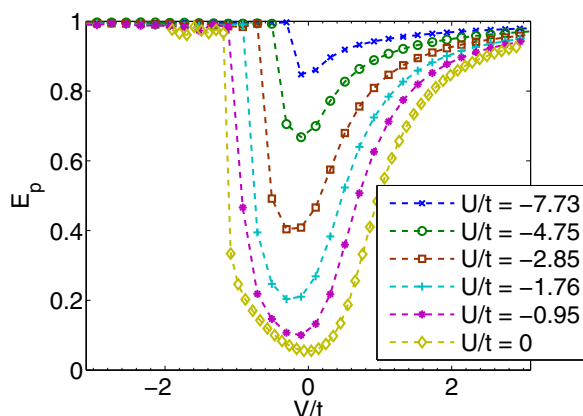


FIG. 5. (Color online) Entanglement behavior across the PS-SS-CDW phases. The entanglement, for any fixed attractive on-site interaction (U/t), is characterized by a discontinuity (PS-SS transition), followed by a local minimum (SS-CDW transition).

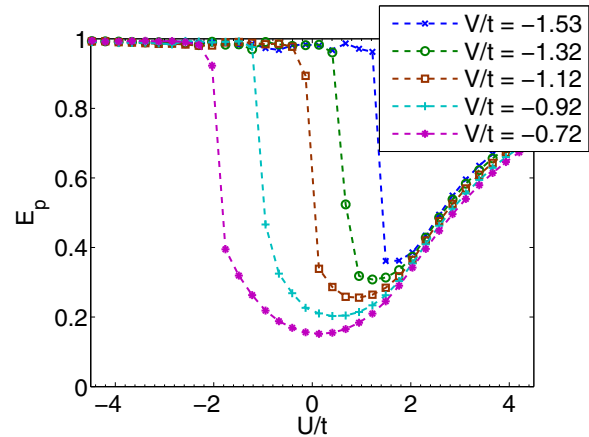


FIG. 6. (Color online) Entanglement behavior across the PS-TS-SDW phases. The entanglement, for any fixed attractive intersite interaction (V/t), is characterized by a discontinuity (PS-TS transition), followed by a local minimum (TS-SDW transition). For large V/t , the two transitions shrink at the same point, and there is no TS phase anymore.

however, that the SS-CDW transition is not located exactly at $V/t = 0$, as expected from the phase diagram described in the literature, but at a value close to this one. We believe that this discrepancy is related to finite-size effects.

B. PS-TS-SDW

In Fig. 6, we see the entanglement behavior across the PS-TS-SDW phases. We see again the two kinds of behavior for any fixed attractive intersite interaction ($V/t < 0$): a first discontinuity, related to the first-order transition PS-TS, followed by a local minimum point related to the second-order transition TS-SDW. Note that, for large values of the attractive intersite interaction, $V/t \simeq -1.5$, the discontinuity and minimum converge to the same point, and there is no TS phase anymore.

C. PS-SDW-(BOW)-CDW

In Fig. 7, we see the entanglement behavior across the PS-SDW-BOW-CDW phases. We see that, as we increase the value of the intersite interactions, for any fixed repulsive on-site interactions ($U/t > 0$), the entanglement identifies two transitions. Firstly, we see a discontinuity, related to the first-order transition PS-SDW, followed then by (i) a discontinuity, when considering large U/t or (ii) a local minimum point, when considering small U/t . Such discontinuity is related to the first-order SDW-CDW transition, while the minimum points are related to the second-order BOW-CDW transition (the SDW-BOW transition is not seen, as aforementioned). We see that the transitions to the CDW phase occur at $U \approx 2V$. Performing a finite-size scaling analysis (see Appendix), we obtain that, for $U/t = 4$, the BOW-CDW transition is located at $V/t = 2.11 \pm 0.01$, which is slightly lower than the literature results, namely $V/t \approx 2.16$ [11,12,15,16].

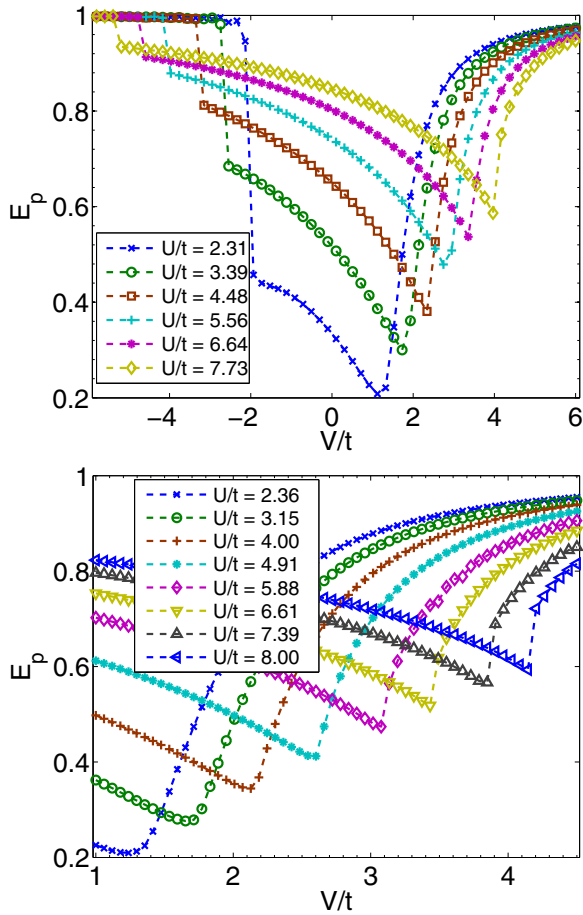


FIG. 7. (Color online) Entanglement behavior across the PS-SDW-BOW-CDW phases. The bottom panel is a magnification of the top panel in the region $1 \leq V/t \leq 4.5$. The entanglement, for any fixed repulsive on-site interaction (U/t), is characterized by a discontinuity (PS-SDW transition), followed by (i) a discontinuity for large V/t (SDW-CDW transition) or (ii) local minimum points for small V/t (BOW-CDW transition).

V. CONCLUSION

We studied the entanglement of indistinguishable particles in the extended Hubbard model at half-filling, with focus on its behavior when crossing the quantum phase transitions. Our results showed that the entanglement either has discontinuities, or presents local minima, at the critical points. We identified the discontinuities as first-order transitions, and the minima as second-order transitions. In this way, we concluded that the entanglement of particles can “detect” all transitions of the known diagram, except for the subtle transitions between the superconductor phases TS-SS, and the transition SDW-BOW.

It is also interesting to compare our results with other entanglement measures, such as the entanglement of modes, which was widely studied in several models, as well as in the extended Hubbard model [37–39]. Gu *et al.* [38] firstly showed that the entanglement of modes, i.e., the entanglement of a single site with the rest of the lattice, could detect three main symmetry broken phases, more specifically, the CDW, SDW, and PS. Other phases were not identified due to the fact that they are associated to off-diagonal long-range order. Further investigations were performed analyzing the

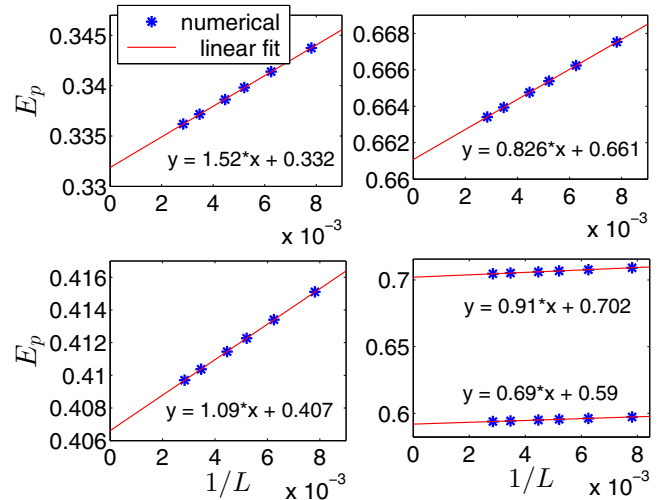


FIG. 8. (Color online) Scaling of the entanglement at the SDW-BOW-CDW phase transitions. For a fixed parameter $U/t = 4$, we have (upper left) minimum entanglement critical point $(V/t)_c = 2.11$; (upper right) $V/t = (V/t)_c + 0.5$; (bottom left) $V/t = (V/t)_c - 0.5$. For a fixed $U/t = 8$ (bottom right), there is a discontinuity in the entanglement, highlighted by the scaling at $V/t = 4.147$ (bottom curve), and $V/t = 4.153$ (upper curve).

block-block entanglement [37,39], i.e., the entanglement of a block with l sites with the rest of the lattice ($L-l$ sites), showing that this more general measure could then detect the transition to the superconducting phase, as well as the bond-order phase. The measure, however, could not detect the SS-TS transition, besides presenting some undesirable finite-size effects in the PS phase. On the other hand, the entanglement of particles

TABLE I. Scaling constants for the entanglement, $E_p = aL^{-1} + E_p(L \rightarrow \infty)$, at different points of the phase diagram, as highlighted in Fig. 3. The symbol “*” denotes the critical points, and “–” means that the entanglement is constant, apart from numerical inaccuracy, for the analyzed lattices. The estimated error for E_p and a is of the order of $\mathcal{O}(10^{-3})$.

U/t	V/t	$E_p(L \rightarrow \infty)$	a
4	1.61	0.407	1.09
4*	2.11*	0.332	1.52
4	2.61	0.661	0.826
8	4.147	0.59	0.69
8	4.153	0.702	0.91
5.723*	3*	0.457	0.911
-1.76	-0.6	0.273	2.41
-1.76*	-0.233*	0.174	3.08
-1.76	0	0.211	2.51
0.4	-1	0.211	2.11
0.67*	-1*	0.204	2.59
2	-1	0.33	2.48
-7.73	-2.55	0.995	–
-7.73	-2.33	0.884	0.69
-2.03	-0.72	0.978	–
-1.875	-0.72	0.403	7.59
3.75	-2.95	0.985	–
4.05	-2.95	0.772	0.439

studied in this work showed no undesirable finite-size effects in the PS phase, but could not detect the superconductor SS-TS transition either. Regarding the BOW phase, from the above discussion we see that it would be worth to analyze more general measures for the entanglement of particles, which goes beyond single-particle information. Some steps in this direction were made in Ref. [18], where a notion of entanglement of “subgroups” of indistinguishable particles was defined.

ACKNOWLEDGMENTS

We acknowledge financial support by the Brazilian agencies FAPEMIG, CNPq, and INCT-IQ (National Institute of Science and Technology for Quantum Information).

APPENDIX: FINITE-SIZE SCALING ANALYSIS

In this appendix, we perform a finite-size scaling analysis in the system entanglement, in order to extract information about the ground state of the model. We obtained that the entanglement behavior is qualitatively the same for lattices larger than $L \approx 100$, with just small differences of the order of $\mathcal{O}(10^{-2})$ in its magnitude. In a general way, the entanglement scales with the inverse of the lattice size, $E_p = aL^{-1} + b$, where a and b are constants. See in Fig. 8, for example, the entanglement scaling for the SDW-BOW-CDW phase transitions. In Table I, we show the computed values for the scaling constants at different points in the phase diagram, as highlighted in Fig. 3.

-
- [1] L. Amico, R. Fazio, A. Osterloh, and V. Vedral, *Rev. Mod. Phys.* **80**, 517 (2008).
- [2] J. Hubbard, *Proc. R. Soc. Lond. A* **276**, 238 (1963).
- [3] J. Sólymon, *Adv. Phys.* **28**, 201 (1979).
- [4] F. Iemini and R. O. Vianna, *Phys. A. Rev* **87**, 022327 (2013).
- [5] F. Iemini, T. O. Maciel, T. Debarba, and R. O. Vianna, *Quantum Inf. Process.* **12**, 733 (2013).
- [6] F. Iemini, T. Debarba, and R. O. Vianna, *Phys. Rev. A* **89**, 032324 (2014).
- [7] U. Schollwöck, *Ann. Phys.* **326**, 96 (2011).
- [8] B. Bauer, L. D. Carr, H. G. Evertz, A. Feiguin, J. Freire, S. Fuchs, L. Gamper, J. Gukelberger, E. Gull, S. Guertler, A. Hehn, R. Igarashi, S. V. Isakov, D. Koop, P. N. Ma, P. Mates, H. Matsuo, O. Parcollet, G. Pawłowski, J. D. Picon, L. Pollet, E. Santos, V. W. Scarola, U. Schollwöck, C. Silva, B. Surer, S. Todo, S. Trebst, M. Troyer, M. L. Wall, P. Werner, and S. Wessel, *J. Stat. Mech.* (2011) P05001.
- [9] H. Q. Lin, D. K. Campbell, and R. T. Clay, *Chin. J. Phys.* **38**, 1 (2000).
- [10] M. Nakamura, *Phys. Rev. B* **61**, 16377 (2000).
- [11] P. Sengupta, A. W. Sandvik, and D. K. Campbell, *Phys. Rev. B* **65**, 155113 (2002).
- [12] Y. Z. Zhang, *Phys. Rev. Lett.* **92**, 246404 (2004).
- [13] M. D., J. Carrasquilla, L. Taddia, E. Ercolessi, and M. Rigol, *Phys. Rev. B* **91**, 165136 (2015).
- [14] E. Jeckelmann, *Phys. Rev. Lett.* **89**, 236401 (2002).
- [15] Satoshi Ejima and S. Nishimoto, *Phys. Rev. Lett.* **99**, 216403 (2007).
- [16] A. W. Sandvik, L. Balents, and D. K. Campbell, *Phys. Rev. Lett.* **92**, 236401 (2004).
- [17] A. P. Balachandran, T. R. Govindarajan, A. R. de Queiroz, and A. F. Reyes-Lega, *Phys. Rev. Lett.* **110**, 080503 (2013); *Phys. Rev. A* **88**, 022301 (2013).
- [18] G. C. Ghirardi, L. Marinatto, and T. Weber, *J. Stat. Phys.* **108**, 49 (2002).
- [19] G. C. Ghirardi and L. Marinatto, *Phys. Rev. A* **70**, 012109 (2004).
- [20] J. Schliemann, D. Loss, and A. H. MacDonald, *Phys. Rev B* **63**, 085311 (2001); J. Schliemann, J. I. Cirac, M. Kus, M. Lewenstein, and D. Loss, *Phys. Rev. A* **64**, 022303 (2001).
- [21] K. Eckert, J. Schliemann, D. Bruss, and M. Lewenstein, *Ann. Phys.* **299**, 88 (2002).
- [22] Y. S. Li, B. Zeng, X. S. Liu, and G. L. Long, *Phys. Rev. A* **64**, 054302 (2001).
- [23] H. Barnum, E. Knill, G. Ortiz, R. Somma, and L. Viola, *Phys. Rev. Lett.* **92**, 107902 (2004).
- [24] Rolando Somma, Gerardo Ortiz, Howard Barnum, Emanuel Knill, and Lorenza Viola, *Phys. Rev. A* **70**, 042311 (2004).
- [25] P. Zanardi, *Phys. Rev. A* **65**, 042101 (2002).
- [26] H. M. Wiseman and J. A. Vaccaro, *Phys. Rev. Lett.* **91**, 097902 (2003).
- [27] M. C. Banuls, J. I. Cirac, and M. M. Wolf, *Phys. Rev. A* **76**, 022311 (2007).
- [28] F. Benatti, R. Floreanini, and U. Marzolino, *Ann. Phys.* **325**, 924 (2010).
- [29] J. Grabowski, M. Kus and G. Marmo, *J. Phys. A: Math. Theor.* **44**, 175302 (2011); **45**, 105301 (2012).
- [30] T. Sasaki, T. Ichikawa, and I. Tsutsui, *Phys. Rev. A* **83**, 012113 (2011).
- [31] R. Paskauskas and L. You, *Phys. Rev. A* **64**, 042310 (2001).
- [32] A. R. Plastino, D. Manzano, and J. S. Dehesa, *Europhys. Lett* **86**, 20005 (2009).
- [33] C. Zander and A. R. Plastino, *Phys. Rev. A* **81**, 062128 (2010).
- [34] A. Reusch, J. Sperling, and W. Vogel, *Phys. Rev. A* **91**, 042324 (2015).
- [35] R. G. Parr and W. Yang, *Density Matrices: The N-Representability of Reduced Density Matrices. In: Density-Functional Theory of Atoms and Molecules*, The International Series of Monographs on Chemistry Vol. 16 (Oxford University, New York, 1989).
- [36] T. Giamarchi, *Quantum Physics in One Dimension* (Oxford University Press, New York, 2004).
- [37] C. Mund, Ö. Legeza, and R. M. Noack, *Phys. Rev. B* **79**, 245130 (2009).
- [38] Shi-Jian Gu, Shu-Sa Deng, You-Quan Li, and Hai-Qing Lin, *Phys. Rev. Lett.* **93**, 086402 (2004).
- [39] Shu-Sa Deng, Shi-Jian Gu, and Hai-Qing Lin, *Phys. Rev. B* **74**, 045103 (2006).